Acta Materialia Transylvanica 7/1. (2024) 01–07.
DOI: Hungarian: https://doi.org/10.33923/amt-2024-01-01
English: https://doi.org/10.33924/amt-2024-01-01

ACTA MATERIALIA TRANSYLVANICA

Microstructural Characterization of 1.4542 Type Stainless Steel Specimens Manufactured by Fused Filament Fabrication

Adrián BOGNÁR,[1*] György LEDNICZKY,[1] Krisztián KUN,[1] László ZSIDAI[2]

[1*] *John von Neumann University, GAMF Faculty of Engineering and Computer Science, Department of Innovative Vehicles and Materials, Kecskemét, Hungary, bognar.adrian@nje.hu*

[2] *Hungarian University of Agriculture and Life Sciences, Szent István Campus, Institute of Technology, Department of Materials Science and Engineering Processes, Gödöllő, Hungary*

Abstract

The processes of design and manufacturing continue to expand with extraordinary opportunities due to the emergence and development of additive manufacturing technologies. Additive manufacturing processes radically differ from traditional manufacturing methods and require a completely new engineering approach. As a result, new possibilities emerge, allowing the creation of geometries that were previously difficult or impossible to produce using other technologies. Significant application opportunities exist in fields such as medicine and many sectors of industry due to this advancement. The range of materials used in additive manufacturing is constantly improving and expanding, although the most significant results are in the area of industrial applicability, which is the focus of this research. It is important to mention that besides Selective Laser Sintering / Selective Laser Melting (SLS / SLM), Fused Filament Fabrication (FFF) is worth considering for producing metal parts, due to lower costs and the possibility of manufacturing larger parts. The aim of the research is to examine the microstructural and macrostructural characteristics of finished components produced by FFF.

Keywords: *additive manufacturing, material extrusion, stainless steel, microstructural characterization.*

1. Introduction

Additive manufacturing of metal products is increasingly common in the production of automotive parts and medical prosthetics, thanks to a wide range of processes and materials. These processes require significant investment and complex equipment to ensure the safe handling of metal powder with minimal health risks. The metal powders used in processes branded as SLS® (Selective Laser Sintering) or DMLS (Direct Metal Laser Sintering) have particle sizes ranging from 15 to 50 µm, posing similar health risks to operators as welding [1, 2]. Among other reasons, these health risks, along with the substantial investment costs and laser-related safety concerns, have spurred multiple research directions that employ new methods for the additive manufacturing of metal parts [3].

1.1. Additive Manufacturing of metal materials

Among the seven types of additive manufacturing processes defined by the ISO 52900-1 terminology standard, one variant of material extrusion is fused filament fabrication (FFF). The first step in filament-based metal printing involves producing green parts. These components have not yet undergone the debinding and sintering processes. While they are accurate in shape and size, their surface roughness and density are not as well regulated as in laser processes. After the debinding process, the green parts require the most attention and are referred to as brown parts due to their characteristic color at this stage. These parts are porous, brittle, and lack the binder that helps hold them together. According to previous literature reviews, this process has limitations due to

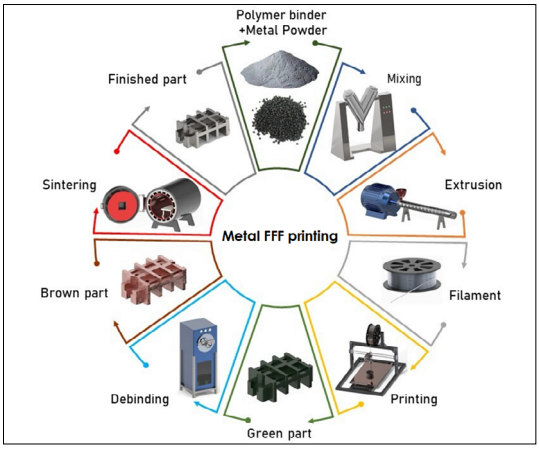

Fig. 1. *The process of metal FFF printing.*

the strength of the test specimens, as the internal parts require a minimum level of infill [1, 3].

The FFF process is simple to perform and requires minimal investment compared to other additive manufacturing processes. Another advantage is that when producing complex parts, there is no need to create channels to remove unused powder from the work area [4, 5, 6].

Figure 1. illustrates the process of producing metal parts based on filament-based technology.

1.2. Post-processing techniques

As mentioned in the previous paragraph, the green parts produced in this way require further treatments to obtain test specimens with properties nearly identical to those made from solid materials [1, 3].

During these treatments, the first step is to remove the binder. The resulting brown parts must then be sintered at high temperatures. If necessary, additional processes, such as heat treatment or hot isostatic pressing, can be performed to enhance mechanical properties [4, 5].

There are three main methods for binder removal:

- solvent-based: using trichloroethane or heptane;
- thermal: applying a temperature range of 60-600°C;
- catalytic: using nitric acid or oxalic acid at temperatures between 110-150°C [7].

After binder removal, the brown parts reach their final state through high-temperature sintering, undergoing a shrinkage of 10–20% compared to the green part. To compensate for this, it is crucial to focus on appropriate scaling settings during the design phase. The dimensions of the test specimens need to be increased to varying extents in the X, Y, and Z directions. The necessary values are provided by the manufacturer of the filler material [8].

During sintering, six mechanisms of material transport are distinguished:

- surface diffusion;
- lattice diffusion;
- grain boundary diffusion;
- evaporation and condensation;
- viscous flow;
- plastic flow [9].

After the sintering process, the porosity of the workpieces is expected to be between 10–20%, depending on the temperature applied. Nitrogen, argon, and hydrogen can be used as protective gases during sintering. Several factors influence the sintering process:

- heating rate;
- sintering temperature;
- sintering process duration;
- furnace atmosphere [10].

2. The methodology of the experiment

The printing was done using BASF Ultrafuse 17-4PH filament. This type of filler material is one of the most common in metal printing literature. Essentially, it is a composite filament produced by extruding a blend of 1.4542 grade stainless steel powder and a binder. The key characteristics related to the processing conditions of this printing filler material are shown in **Table 1.**

Table 1. *Recommended processing parameters for BASF Ultrafuse 17-4PH filament* [8]

Recommended processing parameters	
Nozzle temperature	230–250 °C
Bed temperature	90–100 °C
Nozzle diameter	≥0,4 mm
Printing speed	15–50 m/s
Cooling	nem
Scaling of specimens	X and Y direction: 119% Z direction: 122%

To produce the green parts, we used a Craft-Bot Flow Idex XL 3D printer operating on filament-based technology.

2.1. The modified manufacturing paramters

During the experiment, test specimens commonly used in Metal Injection Molding (MIM) were printed with modified settings [11].

Each piece was printed with 100% infill and oriented in the X-Y plane. Three parameters were selected as variables in the CraftWare slicing software, based on previous literature findings, which could impact mechanical properties and printing time:

– layer thickness (mm);
– printing speed (mm/s);
– infill orientation (°) [12, 13, 14].

Printing speed fundamentally affects the movement speed of the printer head, thus influencing printing time. However, it may also influence the degree of adhesion between layers, potentially affecting tensile strength [15, 16, 17].

Preliminary experiments indicated that printing speed needed to be reduced, so its values had to be chosen from a lower range.

Table 2. *The various printing parameters used for manufacturing the test specimens*

Experiment	Layer height (mm)	Printing speed (mm/s)	Infill orientation (°)
#1	0,2	25	45
#2	0,3	15	45
#3	0,4	35	45

The green part is shown in the Figure 2.

2.2. Binder removal and sintering

Materials composed of different metal powders and binder systems require varied binder removal and sintering technologies and atmospheres, so in this exepriment we enlisted the services of Elnik System GmbH [18].

In the binder removal cycle, the specimens are initially preheated to 120 °C at a low heating rate. Initially, the rate is set to 5 °C, then reduced to 1 °C, and finally to 0.5 °C per minute. Once 120°C is reached, they are held at this temperature for 45 minutes. Subsequently, the acid flow begins, lasting for one hour per 1 mm of wall thickness. The flow rate of the acid is 3.4 ml per minute. After the acid flow is complete, the specimens are held at 120 °C for 90 minutes to clean the furnace and prepare for opening.

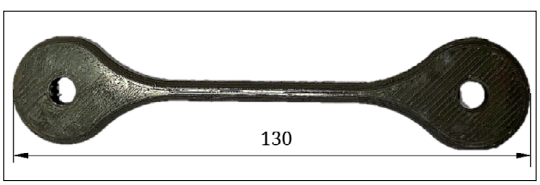

Fig. 2. *The manufactured green part.*

The binder removal process is illustrated in the Figure 3.

CD 3045 furnace (Figure 4) is used for removing the Catamold binder system patented by BASF.

After binder removal, sintering takes place in a different apparatus. The sintering cycle (Figure 5) begins with a re-binder removal phase. Initially, the temperature is raised to 450°C at a rate of 5°C per minute, and then held at this temperature for 150 minutes.

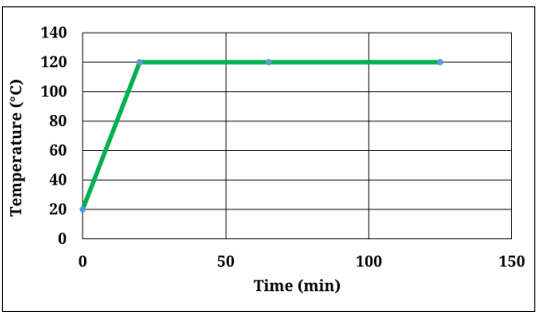

Fig. 3. *Diagram of the binder removal process.*

Fig. 4. *CD 3045 binder removal furnace.* [18]

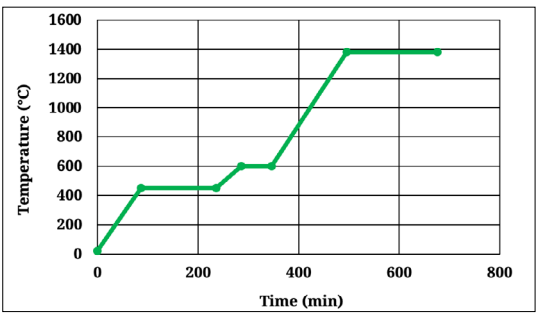

Fig. 5. *Diagram of the sintering process.*

The next step involves heating to 600°C at a rate of 3°C per minute and holding it for 60 minutes. Sintering occurs at 1380°C, reached at a heating rate of 5°C per minute, and held for 180 minutes. Finally, the furnace is allowed to cool freely to room temperature.

The MIM 3045 sintering furnace is shown in the **Figure 6.**

The finished specimen (**Figure 7**) with metallic properties after binder removal and sintering.

3. Results and evaluations

The following imaging techniques offer various advantages, enabling detailed analysis of the structure and composition of test specimens. The electron microscope produces high-resolution images, revealing fine details at nearly nanometer levels. The confocal microscope allows for the visualization of three-dimensional structures with optical sectioning capability. The light microscope provides a more comprehensive view of the samples, enabling observation of larger-scale features and overall morphology. These imaging methods offer valuable insights into the microstructural characteristics of the samples. The images were taken from test specimens subjected to tensile testing, which is not covered in the current research.

Fig. 6. *MIM 3045 sintering furnace.* **[18]**

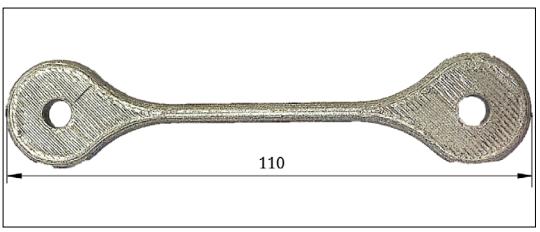

Fig. 7. *The final metal specimen.* **[11]**

3.1. Electron microscopy images

The microstructural examination images were taken using a Zeiss Sigma 300 VP scanning electron microscope (SEM) with a secondary electron (SE) detector. This detector can detect low-energy electrons, allowing for the determination of surface shape and morphology. Additionally, the backscattered electron detector (BSD) provides further assistance by identifying different elements of the periodic table with atomic number sensitivity. The images shown in **Figures 8–10** were taken from the fracture surfaces of the tensile-tested specimens.

Significant porosity is observed on the surfaces of all examined experimental samples. Porosity is influenced by the sintering conditions among other factors. An interesting phenomenon is observed on the sample of Exp. #3, where at lower magnifications, the surface of the layers appears heavily granular, yet at 2000x magnification, it seems less porous compared to the other two samples. It appears that the fusion of layers is more effective with smaller layer thicknesses.

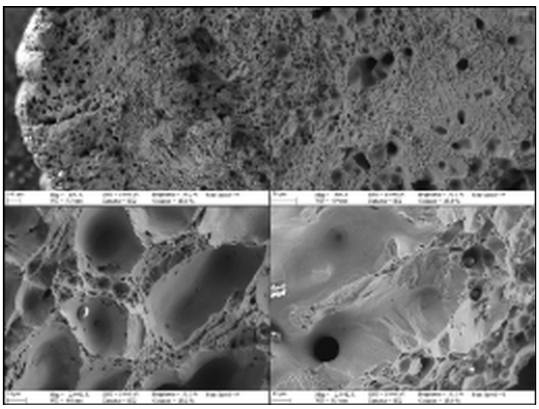

Fig. 8. *Exp. #1 SEM image with SE detector.*

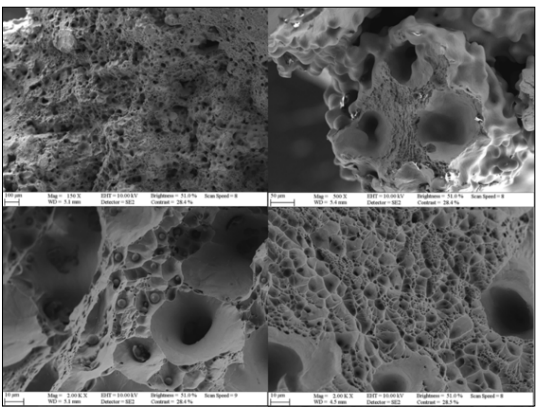

Fig. 9. *Exp. #2 SEM image with SE detector.*

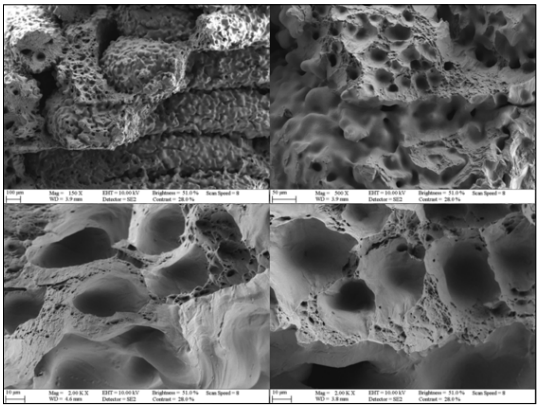

Fig. 10. *Exp. #3 SEM image with SE detector.*

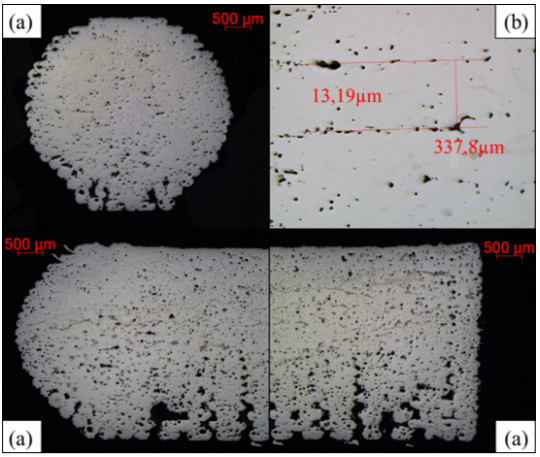

Fig. 11. *Microstructural image of the Exp. #1 specimen in polished condition.*

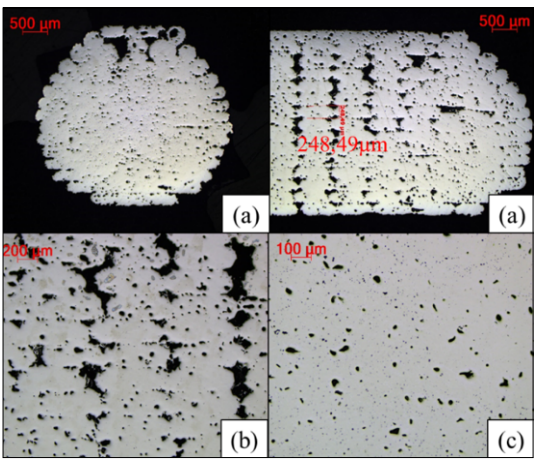

Fig. 12. *Microstructural image of the Exp. #2 specimen in polished condition.*

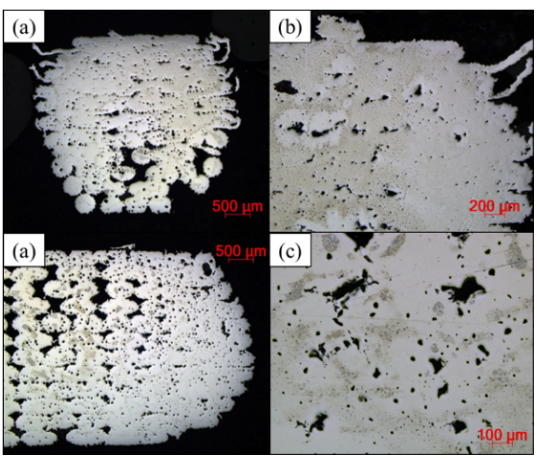

Fig. 13. *Microstructural image of the Exp. #3 specimen in polished condition.*

3.2. Polished specimen sections under a light microscope

Embedded polished samples were prepared from the experiments. After polishing, the samples were analyzed using a Zeiss Axio Imager M.2m microscope. Microscopic examination allows for a comparison between the polished section and the fracture surface, with particular attention to the porosity and material continuity defects visible in the SEM images.

After polishing, images of the samples were taken. **Figures 11–13.** show the samples from each experiment at 25, 50 and 100× magnifications.

In Exp. #1, larger material continuity defects are observed in the initial layers, which can be attributed to the green product and, consequently, to the printing process. Although the layers mostly fused well in the inner part of the cross-section after sintering, layering is still noticeable on the outer surface (shell).

A similar observation can be made for the sample from Exp. #2, with the difference that the individual layers and weaker layer fusion are more visible in the cross-section taken from the head along the hole.

In Exp. #3, the initial layer defects are also visible, and larger material continuity defects are seen along the layers in the sample taken along the hole.

At both lower and higher magnifications, significant porosity is evident in all test specimens.

3.3. Etched and polished specimen sections under a confocal microscope

The confocal microscope creates a virtual plane through optical imaging. It can produce high-quality images with fine details and greater contrast

than traditional microscopes. Additionally, this imaging technique allows for the reconstruction of virtual three-dimensional images of the examined object. The microscopic images were taken using an Olympus OLS5000-SAF confocal microscope. The images captured with the confocal microscope are shown in **Figures 14–16.**

The yellowish-brown hue visible in the images is caused by the residue of the etchant remaining on the polished surface. For etching the polished sections (since the material of the sample is stainless steel) a solution called aqua regia were used, composed of:

- 10 ml nitric acid;
- 20 ml hydrochloric acid;
- 30 ml water.

The etchant was applied to the samples using a pipette, left on for 1 minute, then rinsed with water and cleaned with alcohol before drying.

The microstructures visible in the images exhibit minor variations but are generally consistent. Porosity, as observed with the light microscope, is consistently present in all experimental samples.

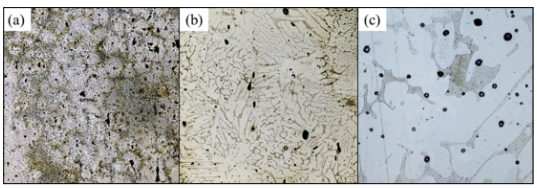

Fig. 14. *Microstructural image of the Exp. #1 specimen in etched condition.*

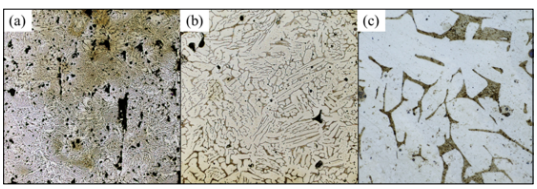

Fig. 15. *Microstructural image of the Exp. #2 specimen in etched condition.*

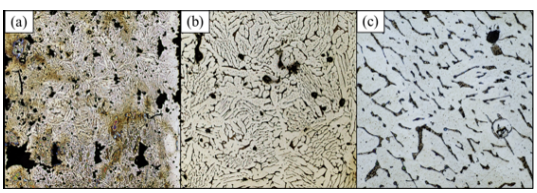

Fig. 16. *Microstructural image of the Exp. #3 specimen in etched condition.*

4. Conclusions

The microscopic polished samples presented in this research are part of the findings from a more extensive study. The images clearly show that the produced test specimens exhibit significant porosity. It is also observed that processing parameters have a substantial impact on the resulting micro- and macrostructure. These cavities and pores are well-visualized in the electron microscopy images. Micro- and macrostructural defects significantly reduce the achievable mechanical properties of materials produced through additive manufacturing. Therefore, defining the optimal printing strategy and parameters to achieve the best and most homogeneous products is of paramount importance. The defects identified during the research open up opportunities for further studies, such as evaluating the effectiveness of binder reduction and detailed analysis of the effects of sintering parameters.

References

[1] Henry T. C., Morales M. A., Cole D. P., Shumeyko C. M., Riddick J. C.: *Mechanical behavior of 17-4 PH stainless steel processed by atomic diffusion additive manufacturing*. International Journal of Advanced Manufacturing Technology, 114/7–8. (2021) 2103–2114. https://doi.org/10.1007/S00170-021-06785-1/FIGURES/13

[2] Nurhudan A. I., Supriadi S., Whulanza Y., Saragih A. S.: *Additive manufacturing of metallic based on extrusion process: A review.* Journal of Manufacturing Processes, 66. (2021) 228–237. https://doi.org/10.1016/J.JMAPRO.2021.04.018

[3] Zhang Y., Roch A.: *Fused filament fabrication and sintering of 17-4PH stainless steel.* Manufacturing Letters, 33. (2022) 29–32. https://doi.org/10.1016/J.MFGLET.2022.06.004

[4] Kedziora S., Decker T., Museyibov E., Morbach J., Hohmann S., Huwer A., Wahl M.: *Strength Properties of 316L and 17-4 PH Stainless Steel Produced with Additive Manufacturing*. Materials, 15. 15/18. 6278. https://doi.org/10.3390/MA15186278

[5] Vaschetto S., Filipe J., Fernandes P., Selema A., Ibrahim M. N., Sergeant P.: *Metal Additive Manufacturing for Electrical Machines: Technology Review and Latest Advancements*. Energies 15/3. (2022) 1076. https://doi.org/10.3390/EN15031076

[6] Cho Y. H., Park S. Y., Kim J. Y., Lee K. A.: *17-4PH stainless steel with excellent strength–elongation combination developed via material extrusion additive manufacturing.* Journal of Materials Research and Technology, 24. (2023) 3284–3299.

[7] Molaei R., Fatemi A., Phan N.: *Multiaxial fatigue*

of LB-PBF additive manufactured 17–4 PH stainless steel including the effects of surface roughness and HIP treatment and comparisons with the wrought alloy. International Journal of Fatigue, 137. (2020) 105646. https://doi.org/10.1016/J.IJFATIGUE.2020.105646

[8] Techinical Datasheet 17-4 PH https://forward-am.com/wp-content/uploads/2021/02/Ultrafuse_17-4PH_TDS_EN_v1.1.pdf (accessed on:: 2024. 03. 13.)

[9] Pellegrini A., Lavecchia F., Guerra M. G., Galantucci L. M.: *Influence of aging treatments on 17–4 PH stainless steel parts realized using material extrusion additive manufacturing technologies.* International Journal of Advanced Manufacturing Technology, 126/1–2. (2023) 163–178. https://doi.org/10.1007/S00170-023-11136-3/TABLES/6

[10] Nurhudan A. I., Supriadi S., Whulanza Y., Saragih A. S.: *Additive manufacturing of metallic based on extrusion process: A review.* Journal of Manufacturing Processes, 66. (2021) 228–237. https://doi.org/10.1016/J.JMAPRO.2021.04.018

[11] Sidambe A. T., Figueroa I. A., Hamilton H. G., Todd I.: *Taguchi optimization of MIM titanium sintering.* International Journal of Powder Metallurgy, 47/6. (2011) https://openurl.ebsco.com/EPDB%3Agcd%3A6%3A13675718/detailv2?sid=ebsco%3Aplink

[12] Singh G., Missiaen J. M., Bouvard D., Chaix J. M.: *Additive manufacturing of 17–4 PH steel using metal injection molding feedstock: Analysis of 3D extrusion printing, debinding and sintering.* Additive Manufacturing, 47. (2021) 102287. https://doi.org/10.1016/J.ADDMA.2021.102287

[13] Spiller S., Kolstad S. O., Razavi, N.: *Fabrication and characterization of 316L stainless steel components printed with material extrusion additive manufacturing.* Procedia Structural Integrity, 42. (2022) 1239–1248. https://doi.org/10.1016/J.PROSTR.2022.12.158

[14] Chemkhi M., Djouda J. M., Bouaziz M. A., Kauffmann J., Hild, F., Retraint, D.: *Effects of Mechanical Post-Treatments on Additive Manufactured 17-4PH Stainless Steel Produced by Bound Powder Extrusion.* Procedia CIRP, 104. (2021). 957–961. https://doi.org/10.1016/J.PROCIR.2021.11.161

[15] Liu B., Wang Y., Lin Z., & Zhang T.: *Creating metal parts by Fused Deposition Modeling and Sintering.* Materials Letters, 263. (2020) 127252. https://doi.org/10.1016/J.MATLET.2019.127252

[16] Maj P., Adamczyk-Cieslak B., Lewczuk M., Mizera J., Kut S., Mrugala T.: *Formability, Microstructure and Mechanical Properties of Flow-Formed 17-4 PH Stainless Steel.* Journal of Materials Engineering and Performance, 27/12. (2018) 6435–6442. https://doi.org/10.1007/S11665-018-3724-9/TABLES/4

[17] Sadaf M., Bragaglia M., Nanni, F.: *A simple route for additive manufacturing of 316L stainless steel via Fused Filament Fabrication.* Journal of Manufacturing Processes, 67. (2021) 141–150. https://doi.org/10.1016/J.JMAPRO.2021.04.055

[18] https://elnik.com/products/ (accessed on: 2024. 03. 13.)